Proceedings World Geothermal Congress 2000
Kyushu - Tohoku, Japan, May 28 - June 10, 2000

NEW DEVELOPMENT OF 3-D STOCHASTIC MODEL FOR DESIGN OF HDR/HWR GEOTHERMAL RESERVOIRS SYSTEM

Ayumu Shimizu[1], Toshiyuki Hashida[1], Kimio Watanabe[2] and Jonathan Willis-Richard[3]
[1] Research Institute Fracture Technology, Tohoku University01 Aza-Aoba, Aramaki, Aoba-ku, Sendai, 980-8579 Japan
[2] RichStone Ltd. Time24 Bldg. 4F 2-45 Aomi, Koto-ku, Tokyo, 135-8073, Japan
[3] Loeb Aron & Company Ltd. Georian House, 63, Coleman strees, London, EC2R 5BB, UK

Keywords: stimulation, simulation, reservoir expansion, Soultz, HDR, HWR

ABSTRACT

The creation of Hot Dry Rock (HDR) / Hot Wet Rock (HWR) [Takahashi and Hashida, 1992] reservoir systems is critical for development of next-generation geothermal energy extraction methodology. HDR/HWR geothermal systems may be engineered in naturally fractured but weakly permeable hard rocks by hydraulic stimulation. The stimulation involves pumping high-pressure fluid injection into the fractured hot rock, which creates a man-made geothermal reservoir with increased permeability. The design of HDR/HWR geothermal systems requires development of simulation models predicting the extension behavior of hydraulically induced fractures.

In this paper, an improved three-dimensional simulation model, based on FRACSIM-3D, is presented, which incorporates the mechanical rock-fluid interaction during hydraulic stimulation, in more rigorous way than the existing two-dimensional model FRACSIM-2D, and quantitatively predict the reservoir growth behavior. In this model, pre-existing fractures are generated stochastically, and their radius distribution is assumed fractal. The fluid flow throw the discrete fracture network is solved by converting it to an equivalent continuum mesh under constant injection pressure. The fluid flow is approximated as Darcy type flow, and the pressure distribution within the fracture is used for the calculation of opening and shear displacements. This requires several complete trial flow solutions, realizing the fracture system anew each time and recalculating the shear displacement using the latest inner fracture pressure. The result of this stimulation simulation using data from the European HDR test site Soultz–sous-forest in France are in good agreement with the existing field data. In addition, the effect of variation of the injection pressure during stimulation on the reservoir extension is simulated with the objective of expanding the reservoir volume.

1. INTRODUCTION

In order to understand, design and create a reservoir, many numerical models have been developed and applied to HDR/HWR systems [Lemos and Brady, 1983: Cundall *et al*, 1978: Duteau *et al*, 1994: Swenson *et al*, 1995: Hopkirk *et al*, 1981: Kolditz, 1995: Watanabe and Takahashi, 1995: Bruel *et al*, 1994]. The numerical model FRACSIM-3D developed by the research group in Tohoku University presents a useful model which is capable of simultaneously addressing the problems associated with hydraulic stimulation, fluid circulation and heat extraction [Willis-Richards *et al*, 1996]. In addition, that model takes into account the distribution of natural fractures using a fractal geometry representation, and prescribes the stimulated reservoir dimensions based on acoustic emission monitoring results. The reservoir size that is enlarged by hydraulic stimulation is one of the input data of that model, while the reservoir orientation and shape are predicted based on the rock mechanics principle.

The object of the present work is to create an improved stimulation model that is more rigorous than FRACSIM-2D in describing the mechanical rock-fluid interaction during hydraulic stimulation based on the three-dimensional simulation model FRACSIM-3D. Numerical calculations are performed using this model to clarify the reservoir growth behavior.

2. DESCRIPTION OF THE MODEL

The presented model is a 3-D model, which contains a representation of the fracture network in a cubical rock mass within which a HDR reservoir is developed. The flow properties of a stochastic fracture network that depend on the fluid pressure are mapped onto this regular grid.

2.1 Fractal fracture network

Fractures are generated stochastically within a fracture generation volume of $(L+2r_{max})^3$, where L is the edge length of the model volume and r_{max} is the radius of the largest fracture. The fracture centers obey uniformly random distribution. In a fractal fracture length distribution, the radius of a fracture, r_α, whose characteristic length is specified within lower and upper fracture radius limits (r_{min} and r_{max}), can be expressed as [Willis-Richards *et al*, 1996]:

$$r_\alpha = \left((1-\alpha)r_{\min}^{-D} + \alpha r_{\max}^{-D}\right)^{-1/D} \qquad (1)$$

where α is a random parameter in the interval [0,1], and the D is fractal dimension, which has been proved capable of representing mathematically the geometry of natural fractures [Watanabe and Takahashi, 1995].

The initial (i.e. undisturbed) fracture apertures, a_0, at zero effective stress, are assumed to be proportional to the fracture radius and are expressed as:

$$a_0 = \beta \times r_i \qquad (2)$$

where r_i is the radius of the fracture, and β is a constant of proportionality which is chosen to allow the undisturbed fracture network to match (at least approximately) the in-situ measured permeability [Willis-Richards *et al*, 1996].

For the fracture distribution, which is based on the fracture orientations controlled by field observations made at the HDR/HWR geothermal reservoir, usually from well logs, fractures are generated until the fracture density (m^2 of fracture per m^3 of rock) reaches the observed level.

2.2 Fracture shear dilation behavior

Fracture apertures are affected by both the effective normal stress at the fracture surface and the amount of shear displacement that determines the fit of the opposing rough surfaces.

Shear stability is expressed by a simple friction law, when there is a slip, and:

$$\tau > (\sigma_n - P)\tan\left(i + \phi_{dil}^{eff}\right) \qquad (3)$$

where σ_n is the rock stress normal to the fracture surface, P is the pressure in the fracture and ϕ_{dil}^{eff} is the effective shear dilation angle at a given effective normal stress. The basic friction angle i is a material property of the fracture walls. The effective shear dilation angle ϕ_{dil}^{eff} is a property of both the fracture wall asperities and the effective normal stress

$$f_{dil}^{eff} = \frac{f_{dil}}{1 + 9(s_n - P)/s_{nref}} \qquad (4)$$

where σ_{nref} is the effective normal stress applied to cause a 90% reduction in the compliant aperture. The amount of shear displacement depends on the fracture shear stiffness and on the amount of "excess" shear stress available. Based on elastic theory, shear displacement is expressed as:

$$U = \frac{\tau - (\sigma_n - P)\tan(i + \phi_{dil}^{eff})}{K_s} \quad (5)$$

where U is share displacement, and K_s shear stiffness of the fracture. The change in aperture is a product of the displacement and the tangent of the effective shear dilation angle:

$$a_s = U \tan\left(\phi_{dil}^{eff}\right) \quad (6)$$

An expression for the aperture a of a sheared fracture with unabrading asperities in contact is [Willis-Richards *et al*, 1996]

$$a = \frac{a_0 + U\tan(\phi_{dil})}{1 + 9(\sigma_n - \mathrm{P})/\sigma_{nref}} \quad (7)$$

where a_0 is the initial total compliant aperture of the fracture. Equation (7) provides a simple set of approximate relations that can be used in a model that contains many thousands of fractures, when each of them might undergo a small displacement.

2.3 Stimulation

Stress in the upper crust is typically inhomogeneous, usually with one principal stress approximately normal to the Earth's surface and the other two principal stresses sub horizontal. The present model uses a vertical stress and two horizontal principal stresses, which are taken to be the maximum and minimum principal stresses.

Stimulation, by increasing fluid pressure in a low permeability fractured basement rock volume, causes shear of some of the pressurized existing fractures, which in turn leads to a permanent increase in aperture via shear dilation. The stimulated region is characterized by high permeability, which is surrounded by significantly lower undisturbed permeability region.

Willis-Richards *et al* (1996) has created a simulation code with stimulation using similar theory, and has not taking into account the fluid flow. Correspondingly, reservoir volume and stimulated pressure has been needed as input data, and a linear drop in fluid pressure away from the stimulation injection well to the edge of the stimulated region has been assumed.

However, the stimulated volume responds to injection flow and the maximum reservoir size is determined by the injection constant flow rate. In order to predict the maximum reservoir size, the presented stimulation code calculates the flow distribution during stimulation, the pressure distribution within the field, and then the fracture shear displacement. This stimulation model does not describe the track fluid flow as a function time, instead the fluid flow is calculated in steady state. To solve this problem, in the present are calculated the fluid flow of the loops between fracture aperture and field pressure distribution, and between shear displacement and field pressure distribution. Firstly, the pressure distribution is calculated by iteration, and aperture change responds closely to the local pressures according to equation (7) i.e., to the change of transmissivity with pressure. Then, if the flow rate and the transmissibility change are convergent, the fracture shear displacement is calculated based on equation (3) - (7). By using this method, the maximum reservoir size is determined. A flow chart describing the operation of the model is represented in Figure 1

2.4 Circulation Flow and boundary condition

It is necessary to find steady state flow solutions for this grid at injection pressures lower than those involved in the stimulation, given that the fracture apertures respond to the local pressure through compliance alone equation (7) without further slip. In the flow solutions, the quantity of fluid flow from one block to another is controlled by Darcy's law with the "permeability" contribution of each fracture is proportional to the sum of the products of the third power of the fracture apertures, and the fracture intersection length with the block face. The final steady state flow solution is refined by Gauss-Seidel SOR after Multigrid relaxation.

In the present model, the fluid loss through the boundary is estimated by using a semi-analytic model of compliant fractures with a spherical "fluid dumping" region with the model volume embedded at its central region and bounded externally by fixed pressures. This approach has been used to estimate fluid loss during circulation and stimulation at a number of HDR sites [Willis-Richard, 1995].

3. APPLICATION TO THE SOULTZ FIELD EXPERIMENT

3.1 Field data analysis

An experimental HDR system has been developed in Soultz, France in 1987 with drilled well (GPK-1) with depth of 2002m. In 1988, first stimulation has been performed by injection of 524m^3 of water at a pressure of 6.35MPa into 582m deep open hole. During 1992 - 1993, GPK-1 has been extended from 2002m to 3590m, to obtain higher temperature reservoir. Deep reservoir creation has taken place in 1993 by injecting 25300m^3 water at a maximum effective pressure of approximately 9.25MPa into GPK-1 at a depth from 2850 m to 3400 m. The next stimulation has been carried out by injection of 19300 m^3 of water with a maximum surface pressure of approximately 10MPa at a depth between 2850 m and 3590 m. During 1994 - 1995, borehole GPK-2 has been drilled vertically to 3876m. Furthermore, the first stimulation experiment has been performed by injecting 624m^3 of water at a maximum effective pressure approximately 11.8MPa into GPK-2 at a depth from 3200m to 3876 m. Next stimulation has been carried out with 28000m^3 of water at approximately 12MPa. The seismic locations during these stimulations are shown in Figure 2.

The stress regime in Soultz has been obtained from hydrofarcture stress measurements in GPK-1 and EPS-1. The stress magnitude in Soultz as a function of the depth can be expressed as:

$$S_h = 15.7 + 0.0149(z - 1458) \quad (8)$$
$$S_H = 23.5 + 0.0337(z - 1458) \quad (9)$$
$$S_v = 33.1 + 0.0261(z - 1377) \quad (10)$$

where S_h and S_H are the minor and major horizontal stresses respectively, S_v is the vertical stress due to the weight of the overburden with given rock density, z is the depth in meters, and the stress is measured by MPa. The derived orientation of the maximum horizontal compression θ is N155^{0}E for the depth range between 1458m to 2000m and N170^{0}E for the depth range between 2000m and 3300m. Thus, the ratio of this stress regime changes from $S_h < S_H < S_V$ to $S_h < S_v < S_H$ at the depth of 3000m. This change of the stress regime has a significant effect on the shear growth. Pine and Batchelor (1984) have studied stimulated region growth, using Comborne experiment results. Based on their reports, it can be predicted whether

grows upwards on downwards based on field data, such as main fracture orientation range, total friction angle which is a sum of the basic friction angle i and the dilation component ϕ, and maximum / minimum stresses ratio R. R is expressed as follows:

$$R = \frac{\sigma_1'}{\sigma_3'} = \frac{1+\alpha}{1-\alpha} \tag{11}$$

where α is:

$$\alpha = \frac{\tan\varphi}{\sin 2\theta + \tan\varphi \cos 2\theta} \tag{12}$$

σ_1' and σ_3' are the maximum and minimum principal effective stress respectively, θ is the fracture orientation from the maximum stress, and φ is the total friction angle.

The upward or downward tendency for shear growth at depth z can be expressed as:

$$\text{Upward growth} \qquad \frac{dp_{wd}}{dz} > 0 \tag{13}$$

$$\text{Downward growth} \qquad \frac{dp_{wd}}{dz} < 0 \tag{14}$$

The wellhead pressure p_{wd} required to cause shearing on an existing critically aligned joint at depth z is

$$P_{wd} = \frac{\sigma_1'+\sigma_3'}{2} - \frac{1}{\alpha}\frac{\sigma_1'-\sigma_3'}{2} \tag{15}$$

and its differentiation with respect to z gives:

$$\frac{dp_{wd}}{dz} = \frac{s_1+s_3}{2} - \frac{1}{\alpha}\frac{s_1-s_3}{2} \tag{16}$$

where s_1 and s_3 are local gradients of σ_1' and σ_3' respectively.

Fracture orientation for GPK-1 obtained by a Formation Micro Imager (FMI) is shown in Figure 3. The fracture striking is mainly N010^{0}E and the range of main fracture orientation is from N160^{0}E toN030^{0}E.

Figure 4 shows the values of R as a function of θ, which are determined from equation (11) and (12). The main fracture orientation range delineated from Figure 3 for Soultz field is indicated in Figure 4, along with the values of R at depths of 2000m and 4000m, respectively. This figure indicates that R $\approx$7.8 and $\varphi \approx 50^0$ at the depth of 2000 m, and there might be some shearing fractures with orientations in initial stress regime. Furthermore, the deeper the reservoir, the smaller the stress ratio is, and R $\approx$4.9, and $\varphi \approx 42^0$ at depth of 4000 m. Thus, φ requires 51^0 so as to not slip, and it must keep 42^0 at depth of 4000 m in the case of decreasing dilation angle by normal stress increase.

The condition dp_{wd}/dz>0 has been following solution for the stress regime in Soultz, which is obtained by using equation (16).

$$\varphi > 31.56^0 \qquad (S_v\text{-}S_h) \tag{17}$$

$$\varphi > 40.41^0 \qquad (S_H\text{-}S_h) \tag{18}$$

in which case the reservoir grows upward. The dependence of the critical angle φ_c, which does not shear at hydrostatic pressure in fracture, versus depth is shown in Figure 5. φ_c can also be determined from:

$$\varphi_c = \arcsin\left(\frac{(\sigma_1-\sigma_3)/2}{(\sigma_1+\sigma_3)/2}\right) = \arcsin\left(\frac{\sigma_1-\sigma_3}{\sigma_1+\sigma_3}\right) \tag{19}$$

It is seen from the Figure 5, when φ is larger than φ_c, fractures do not shear in hydrostatic pressure regime. This Figure illustrates that if φ>51^0 at z=2000 m, shear doesn't occur, and the same result is found for the case of φ>42^0 at z = 4000 m in initial pressure regime. Thus, reservoir grows upward during hydraulic stimulation in Soultz, because φ satisfies the criterion dp_{wd}/dz>0. Below depth of the 3000 m, critical angle does not vary significantly with the depth, since the stress regime is S_H-S_h. Nevertheless, for z<3000m the stress regime becomes S_v-S_h, and the critical angle increases when the depth decreases. It appears that a relatively stable reservoir can be created for z>3000m. It is very difficulty to control the creation of reservoir when the depth has to be less than 3000m, otherwise injection pressure should be controlled very well. Acoustic Emission (AE) cloud propagated upward very much during stimulation of GPK-1 experiment. By comparing those at depths deeper than 3000m with shallower than 3000 m, it turns out AE map becomes very small. Open hall of GPK-2 has been located deeper than 3200m, and the AE cloud has propagated upward during the GPK-2 stimulation. However, the upward propagation of the AE cloud during the GPK-2 stimulation has been smaller than during the GPK-1 stimulation. The amount of upward AE cloud propagation is likely to have been affected not only by the permeability distribution around open hole, but also by these stress environment and rock mechanics.

Table 1 shows the most significant model inputs required for simulation of the experimental HDR reservoir system in the Soultz experiment. The calculation region set for the simulation of the Soultz reservoir is 2300x2300x2300m. The center of the modeled region is located at a depth of 3200m. The model contains 96x96x96 finite elements.

3.2 Simulation of the Soultz Field experiment

A simulation result of the stimulation is illustrated in Figure 7. Stimulated fracture center for North-South side view indicates that the reservoir propagates upward and the simulation result is in good agreement with the AE map of the field experiment. During stimulation of GPK-2, the stimulated region propagation is relatively small and does not grow downward. However, we can recognize upward growth of the stimulated region, although it is not as prominent as for GPK-1. This result is in good agreement with the field experiment. It is shown that stimulated region mainly propagates at approximately N010^{0}E in plane view. It also turns out that the stimulated areas between GPK-1 and GPK-2 have only limited connection. However, the experimental results show that the AE clouds have propagated toward N150^{0}E and have overlapped with each other. Corresponding, the simulation results do not correspond to the experimental data. The angle between the main stress and the AE cloud propagation orientation is approximately counterclockwise 20^0 in the experimental data. Moreover, the angle between the propagation stimulated fracture center and the main stress orientation is also approximately clockwise 20^0 in the simulation. The difference between the striking θ and the main stress at the critical angle is shown in Figure 8. Most slippery fracture strike at the critical angle from 20^0 to 24.5^0, which the main stress changes from 2000 m to 4000 m. Therefore, fracture striking of N012^{0}E and N148^{0}E is easy to slip. Figure 3 illustrates that the N012^{0}E striking fracture set prevails over the N148^{0}E set. As a result, the shear orientation of fractures is dominated by the N012^{0}E set, and the stimulated region is expected to grow up towards the N010^{0}E orientation. Jones and Jupe (1997) have analyzed the AE cloud of the stimulation in Soultz. They have reported that, for AE map of plane view, and depths from 2700 m, 2900 m, 3100 m, 3300 m and 3500 m to 2900 m, 3100 m, 3300 m, 3500 m and 3700 m, respectively,

the principal AE propagation near the GPK-1 well has been N010^{0}E from 2700 m to 2900 m. Thus, a plane view of this simulation result is in good agreement with the experimental data obtained for this depth range. The simulated result for the North-South side view of both the stimulated area and the reservoir shape are also in good agreement with the experimental data in rock mechanics. The computed value of the flow rate of the production wells is 17.29 ℓ/sec and of the recovery rate was 71.8%, while the corresponding experimental values are 24 ℓ/sec and 100% respectively. The significant mismatch between these computed and experimental data is expected to be caused by the fact that the shearing propagation orientation is N010^{0}E.

The change of the stimulated region growth with respect to the injection pressure is also investigated. Figure 9 shows the injection pressure versus the change of the stimulated volume for a) GPK-1, b) GPK-2. Figure 9 a) indicates that increasing of the stimulated domain volume for GPK-1 well stimulation from 8 to 9 MPa injection pressure is significant. A map of the stimulated fracture center for injection pressure of 9.5MPa is represented in Figure 10. It does not propagate upward for z<2600m, if the pressure is less than 10MPa. In the case of 10Mpa, which was respected in Figure 7, the stimulated region grows upward significantly. The reservoir reaches the boundary of the calculation field and calculation does not converge for this case, so we abbreviate that data. Nevertheless, the main calculated results are that if the injection pressure exceeds a certain value, the stimulated area propagates explosively and it is difficult to control the propagation. This is in good agreement with the analytics results described at above. Figure 9 b) shows that stimulated domain volume by GPK-2 stimulation increases significantly when the pressure exceeds 10MPa. However, the stimulated region grows overall with upward bias, and it propagates along a particular direction unlike in the case of GPK-1 stimulation. This supports the analytical result discussed above, that for the GPK-2 well the stimulated region does not grow upward as much as for GPK-1 because the stress regime is S_H-S_h.

The propagation of the stimulated region in Soultz-sous-forest simulation computed using the stimulation model and considering that the total friction angle decreases with the depth due to a change in the stress regime is almost equal to the propagation derived from experimental data. These results confirm the validity of the proposed model.

4. Conclusion

A new simulation code of stimulation considering the fluid flow is developed and applied to data from the European HDR test site Soultz-sous-forest. The stimulated results are in good agreement with the experimental data in stimulated region propagation viewing from west. However, the agreement for plane view is insufficient. The reason of this is due to fracture data of GPK-1 FMI. Thus, flow rate and recovery rate are not agreement with experimental data. The simulation of GPK-1 stimulation shows that the stimulated region grows upward and its shape is similar to the experimental one. The main reason for this is that the total friction angle φ is larger than 51^0 at depth of 2000m in our computations. In addition, when the stimulated pressure increases, it turns out that the stimulated region expands. The expanding motion tends to be explosive above a certain pressure, which hampers the controllability of the stimulation reservoir expansion.

REFERENCES

Baria, R., Baumgartner, J., Agerard, A., and Jung, R. (1995). *Results of the stimulation of the second well and first circulation tests at Soultz-sous-Forets*, *Alsace.* HDR geothermal energy project report, Socomine.

Bruel, D., Cacas, M.C., Ledoux, E. and de Marsily, G. (1994). Modeling storage behavior in a fractured rock mass. *Jnl. of Hydrology,* Vol.162, pp.267-278.

Cundall P.A. *et al* (1978). Computer modeling of jointed rock masses. *Technical Report N-78-4*, US Army Engineers Waterways Experiment Station, Vicksburg, Mississippi.

Duteasu, R., Sprecker, T. and Swenson, D.V. (1994). Preventing short-circuiting of flow in Hot Dry Rock systems. *Final report to Swiss National Energy Research Fund on Project No. NEFF 359*, ETH Zurich/Polydynamics Ltd..

Hopkirk, R.J., Sharma, D. and Pralong, P.J. (1981). Coupled advective and conductive heat transfer in analysis of HDR geothermal sources. In: *Numerical Methods in Heat Transfer*, R. W. Lewis, K. Morgan, and O. Zienkiewitz (Ed)., J. Wiley & Sons.

Jones, R.H., and Jupe, A.J. (1997). Microseismic results from the Soultz 1996 experimental programme.

Kolditz, O. (1995). Modeling flow and heat transfer in fractured rocks: conceptual model of a 3D deterministic fracture network. *Geothermics*, Vol.24, pp.451-470.

Lemos, J.V. and Brady, B.H.G. (1983). Stress distribution in a jointed and fractured medium. *in Proc. 24th. US Symposium on Rock Mechanics.*

Pine, R.J., Batchelor, A.S. (1984). Downward migration of shearing in jointed rock during hydraulic injections. *Int. Jnl. Rock Mech. Min. Sci. & Geomech. Abstr.* Vol.21, pp.249-263.

Takahashi, H. and Hashida, T. (1992). New project for Hot Wet Rock geothermal reservoir design concept. *Proceeding of 17th Workshop on geothermal reservoir engineering*, Stanford University, in press

Watanabe, K. and Takahashi, T. (1995). Fractal geometry characterization of the Hot Dry Rock reservoir Stimulations. *Jnl. Geophysical Res.*, Vol.100, B1, pp.521-528.

Willis-Richards, J., Watanabe, K. and Takahashi, H. (1996). Progress toward a Stochastic rock mechanics model of engineered geothermal system. *Jnl. Geophysical Res.*, Vol.101, B8, pp.481-496.

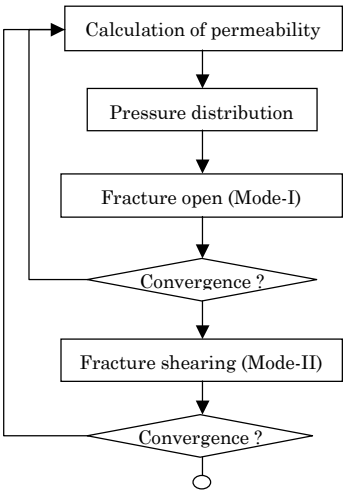

Figure 1: Flow chart of stimulation

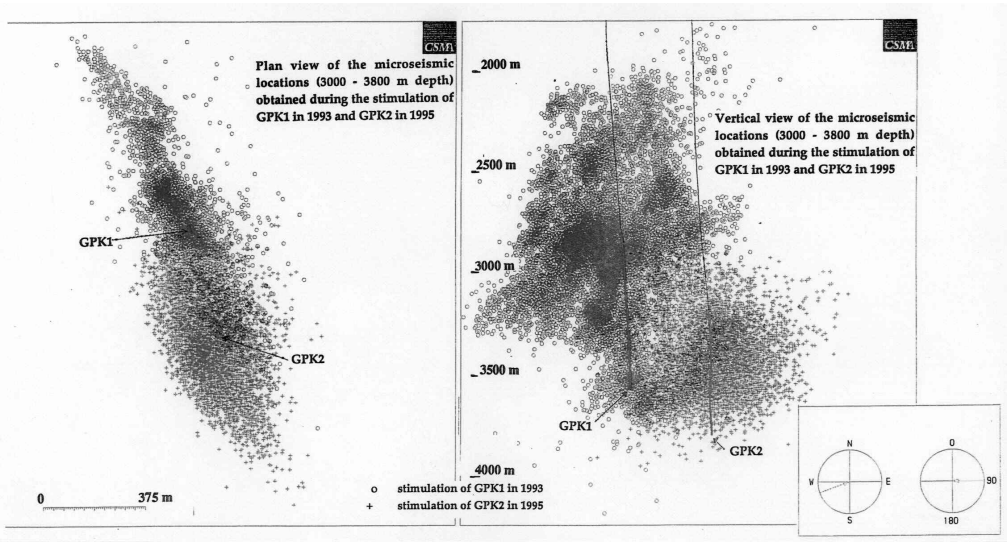

Figure 2: Patterns of microseismicity developed during the stimulations of GPK-1 and GPK-2. the left frame shows the plane view of the clouds and the right frame the horizontal view towards a direction N70^{0}E. Figure from Baria et al.(1995)

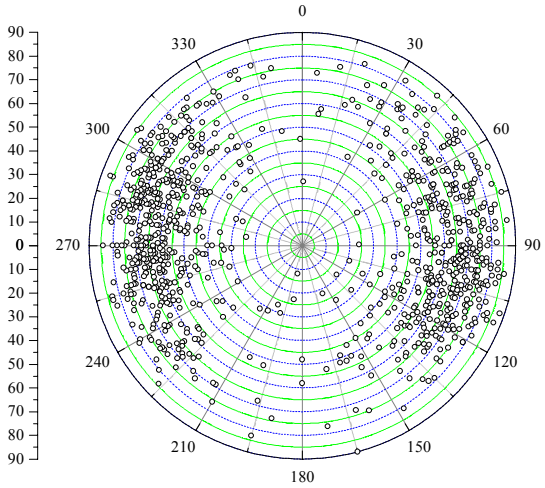

Figure 3: Stereo projection of the fracture poles observed on FMI image of well GPK-1.

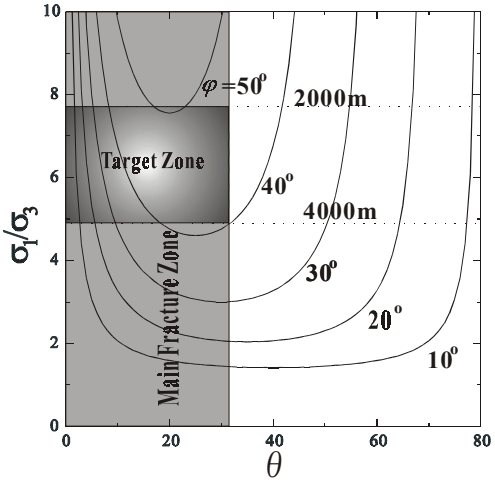

Figure 4: Critical stress ratio and fracture angle from maximum stress. Shadow zone is target of Soultz field. φ is total friction angle.

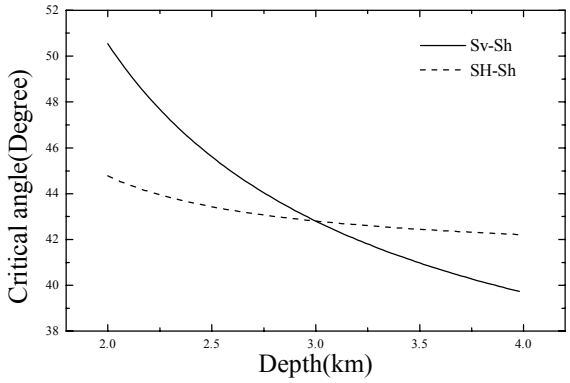

Figure 5: Critical angle φ_c versus depth

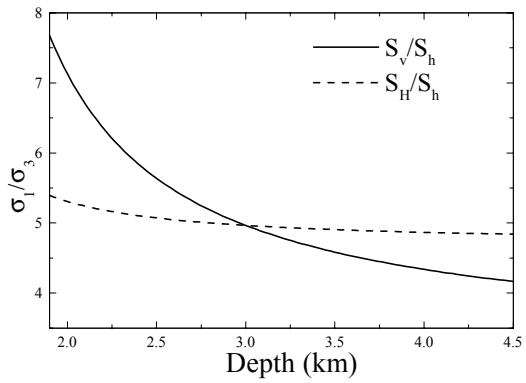

Figure 6: Relationship between stress ratio σ_1/σ_3 and depth

Table 1: Model parameters for HDR simulation at Soultz

Fractal dimension fracture radius	2.0	In situ average permeability (m^2)	$4x10^{-15}$
Fracture density (1/m)	1.5	Fluid viscosity (N s/m^2)	$3x10^{-4}$
Azimuth of maximum horizon	$N170^0E$	Fluid density (kg/m^3)	1000
Young's modules of rock (GPa)	69	Stimulation pressure GPK1 (MPa)	10
Rock poisson's ratio	0.285	GPK2 (MPa)	12.1
Rock Density (kg/m^3)	2660	Circulation pressure GPK1 (MPa)	2.25
Fracture basic friction angle	40^0	GPK2 (MPa)	-3.4
Shear dilation angle	26.5^0	Smallest fracture radius (m)	20
90% closure stress (MPa)	64	Largest fracture radius (m)	250

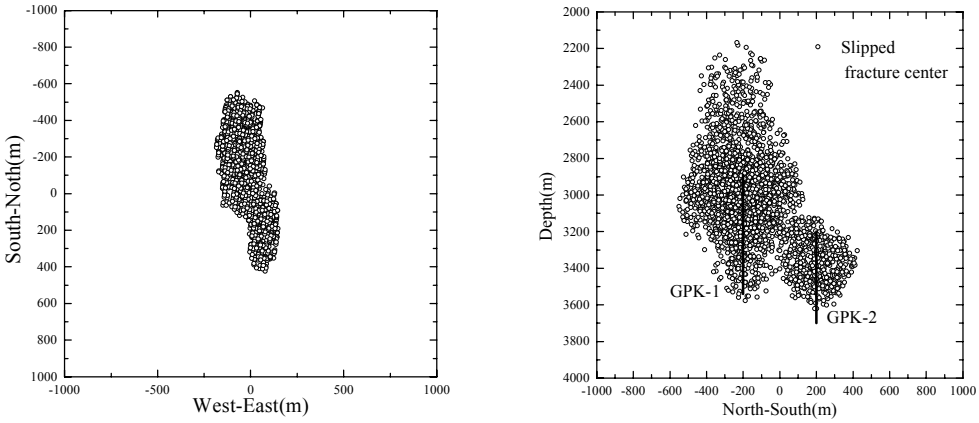

Figure 7: Plane and vertical view of shearing fracture center locations by stimulation simulation. Vertical section viewed from the west.

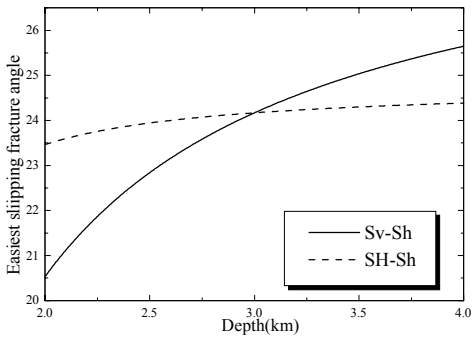

Figure 8: Easiest slipping fracture angle versus depth.

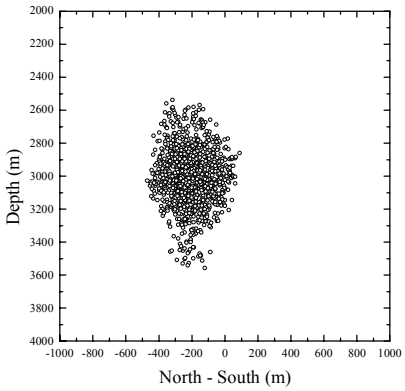

Figure 10: Vertical view of shearing fracture center by GPK-1 stimulation simulation 9.5MPa viewed from the west.

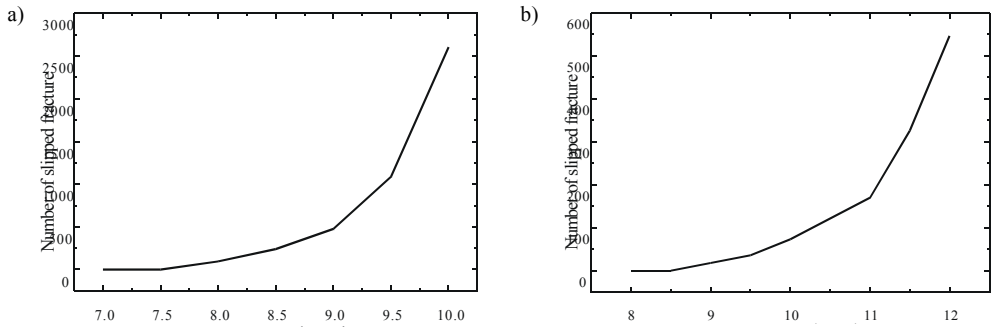

Figure 9: Reservoir expansion behavior at a) GPK-1 and b) GPK-2 stimulation